

Fracture Analyses in Continuously Nonhomogeneous Piezoelectric Solids by the MLPG

J. Sladek¹, V. Sladek¹, Ch. Zhang², P. Solec³ and L. Starek³

Abstract: A meshless method based on the local Petrov-Galerkin approach is proposed for crack analysis in two-dimensional (2-D) and three-dimensional (3-D) axisymmetric piezoelectric solids with continuously varying material properties. Axial symmetry of geometry and boundary conditions reduces the original 3-d boundary value problem into a 2-d problem. Stationary problems are considered in this paper. The axial cross section is discretized into small circular subdomains surrounding nodes randomly spread over the analyzed domain. A unit step function is used as the test functions in the local weak-form. Then, the derived local integral equations (LBIEs) involve only contour-integrals on the surfaces of subdomains. The moving least-squares (MLS) method is adopted for the approximation of the physical quantities in the LBIEs. The accuracy of the present method for computing the stress intensity factors (SIF) and electrical displacement intensity factors (EDIF) are discussed by comparison with available analytical or numerical solutions.

Keyword: Meshless local Petrov-Galerkin method (MLPG), Moving least-squares (MLS) interpolation, piezoelectric solids, functionally graded materials, 2-D and 3-D axisymmetric problems

1 Introduction

Piezoelectric materials have wide range engineering applications in smart structures and devices.

They are extensively utilized as transducers, sensors and actuators in many engineering fields. Piezoelectric ceramics are very brittle and susceptible to fracture during service. To prevent failure, the fracture behaviour of these materials must be well understood. Recently, the study of singular stress and electric fields in cracked piezoelectric materials has attracted the attention of many researchers. Pak (1990) obtained the closed form solutions for an infinite piezoelectric medium under anti-plane loading by using a complex variable approach. Later, Park and Sun (1995) obtained closed form solutions for all three fracture modes for a crack in an infinite piezoelectric medium. They investigated the effect of the electric field on the fracture of piezoelectric ceramics. Shindo et al. (1996, 1997) used an integral transform method to analyze a crack in an infinite piezoelectric strip. Yang and Lee (2001) applied the same method for a penny shaped crack in a three-dimensional piezoelectric strip under in-plane normal loading. Previous analytical approaches were restricted to problems with simple geometry and boundary conditions. Therefore, sophisticated and advanced computational methods like the finite element method (FEM) [Gruebner et al. (2003); Govorukha and Kamlah (2004); Enderlein et al. (2005), Kuna (1998, 2006)] and the boundary element method (BEM) [Pan (1999); Rajapakse and Xu (2001); Davi and Milazzo (2001); Gross et al. (2005, 2007); Garcia-Sanchez et al. (2005, 2007); Saez et al. (2006), Sheng and Sze (2006)] have been applied to general crack analyses in piezoelectric solids.

Functionally graded materials (FGMs) possess continuously nonhomogeneous material properties. These materials have been introduced in recent years to benefit from the ideal performance of its constituents, e.g. high heat and corrosion resis-

¹Institute of Construction and Architecture, Slovak Academy of Sciences, 84503 Bratislava, Slovakia

²Department of Civil Engineering, University of Siegen, D-57068 Siegen, Germany

³Department of Mechanics, Slovak Technical University, Bratislava, Slovakia

tance of ceramics on one side, and large mechanical strength and toughness of metals on the other side. In FGMs, the composition and the volume fraction of their constituents vary continuously with spatial coordinates. A review on various aspects of FGMs can be found in the monograph of Suresh and Mortensen (1998) and the review chapter by Paulino et al. (2003). The demand for piezoelectric materials with high strength, high toughness, low thermal expansion coefficient and low dielectric constant encourages the study of functionally graded piezoelectric materials [Zhu et al. (1995, 1999); Ueda (2003); Han et al. (2006)]. The solution of the boundary value problems for continuously nonhomogeneous piezoelectric solids requires advanced numerical methods due to the high mathematical complexity. Besides this complication, the electric and mechanical fields are coupled each other in piezoelectricity. In spite of the great success of the FEM and BEM as effective numerical tools for the solution of boundary value problems in piezoelectric solids, there is still a growing interest in the development of new advanced numerical methods. In recent years, meshless formulations are becoming popular due to their high adaptability and low costs to prepare input and output data in numerical analysis. A variety of meshless methods has been proposed so far and some of them also applied to piezoelectric problems [Ohs and Aluru (2001); Liu et al. (2002)]. They can be derived either from a weak-form formulation on the global domain or on a set of local subdomains. In the global formulation, background cells are required for the integration of the weak-form. In methods based on local weak-form formulation, no background cells are required and therefore they are often referred to as truly meshless methods. The meshless local Petrov-Galerkin (MLPG) method is a fundamental base for the derivation of many meshless formulations, since trial and test functions can be chosen from different functional spaces. By using the fundamental solution as the test function, accurate numerical results can be obtained, which were reported in previous papers for 2-D problems in isotropic, homogeneous or continuously nonhomogeneous and linear elastic solids under static loading [Atluri et al. (2000);

Sladek et al. (2000); Sellountos et al. (2005)] and for 3-D problems in homogeneous and isotropic solids under static or dynamic loading [Han and Atluri (2004a,b)].

Recently, the MLPG method with a Heaviside step function as the test functions [Atluri et al. (2003); Atluri (2004); Sladek et al. (2004)] has been applied to solve 2-D homogeneous piezoelectric problems [Sladek et al. (2006)]. In the present paper, the MLPG method is extended to 2-D and 3-D axisymmetric continuously nonhomogeneous piezoelectric solids with cracks. The coupled governing partial differential equations are satisfied in a weak-form on small fictitious subdomains. Nodal points are introduced and spread on the analyzed domain and each node is surrounded by a small circle for simplicity, but without loss of generality. For a simple shape of subdomains like circles applied in this paper, numerical integrations over them can be easily carried out. The integral equations have a very simple nonsingular form. The spatial variations of the displacements and the electric potential are approximated by the Moving Least-Squares (MLS) scheme [Belytschko et al. (1996); Zhu et al. (1998)]. After performing the spatial integrations, a system of linear algebraic equations for the unknown nodal values is obtained. The boundary conditions on the global boundary are satisfied by the collocation of the MLS-approximation expressions for the displacements and the electric potential at the boundary nodal points. The accuracy and the efficiency of the proposed MLPG method are verified by several numerical examples for computing the stress intensity factors (SIF) and electrical displacement intensity factor (EDIF). Numerical results are presented and compared with available analytical or numerical solutions.

2 Local boundary integral equations for 2-D problems

Under the static assumption, the governing equations for the mechanical and the electric fields in a continuously nonhomogeneous piezoelectric solid can be written as [Parton and Kudryavtsev

(1988)]

$$\sigma_{ij,j} + X_i = 0, \quad (1)$$

$$D_{j,j} = 0, \quad (2)$$

where σ_{ij} , D_i and X_i denote the stress tensor, the electric displacement and the body force vector, respectively. A comma after a quantity represents the partial derivatives of the quantity.

The constitutive relations representing the coupling of the mechanical and the electrical fields are given by

$$\sigma_{ij}(\mathbf{x}) = c_{ijkl}(\mathbf{x})\varepsilon_{kl}(\mathbf{x}) - e_{kij}(\mathbf{x})E_k(\mathbf{x}), \quad (3)$$

$$D_j(\mathbf{x}) = e_{jkl}(\mathbf{x})\varepsilon_{kl}(\mathbf{x}) + h_{jk}(\mathbf{x})E_k(\mathbf{x}), \quad (4)$$

where $c_{ijkl}(\mathbf{x})$, $e_{jkl}(\mathbf{x})$ and $h_{jk}(\mathbf{x})$ are the elastic, piezoelectric and dielectric material tensors of the continuously nonhomogeneous piezoelectric solids, respectively. The strain tensor ε_{ij} and the electric field vector E_j are related to the displacements u_i and the electric potential ψ by

$$\varepsilon_{ij} = \frac{1}{2}(u_{i,j} + u_{j,i}), \quad (5)$$

$$E_j = -\psi_{,j}. \quad (6)$$

Many piezoelectric solids are transversely isotropic. Under the plane strain condition with $\varepsilon_{33} = \varepsilon_{31} = \varepsilon_{32} = E_3 = 0$, the constitutive equations (3) and (4) are reduced in this case to [Sheng and Sze (2006)]

$$\begin{aligned} & \begin{bmatrix} \sigma_{11} \\ \sigma_{22} \\ \sigma_{12} \end{bmatrix} \\ &= \begin{bmatrix} c_{11} & c_{12} & 0 \\ c_{12} & c_{22} & 0 \\ 0 & 0 & c_{66} \end{bmatrix} \begin{bmatrix} \varepsilon_{11} \\ \varepsilon_{22} \\ 2\varepsilon_{12} \end{bmatrix} - \begin{bmatrix} 0 & e_{21} \\ 0 & e_{22} \\ e_{15} & 0 \end{bmatrix} \begin{bmatrix} E_1 \\ E_2 \end{bmatrix} \\ &= \mathbf{C}(\mathbf{x}) \begin{bmatrix} \varepsilon_{11} \\ \varepsilon_{22} \\ 2\varepsilon_{12} \end{bmatrix} - \mathbf{L}(\mathbf{x}) \begin{bmatrix} E_1 \\ E_2 \end{bmatrix}, \end{aligned} \quad (7)$$

$$\begin{aligned} & \begin{bmatrix} D_1 \\ D_2 \end{bmatrix} \\ &= \begin{bmatrix} 0 & 0 & e_{15} \\ e_{21} & e_{22} & 0 \end{bmatrix} \begin{bmatrix} \varepsilon_{11} \\ \varepsilon_{22} \\ 2\varepsilon_{12} \end{bmatrix} + \begin{bmatrix} h_{11} & 0 \\ 0 & h_{22} \end{bmatrix} \begin{bmatrix} E_1 \\ E_2 \end{bmatrix}, \\ &= \mathbf{G}(\mathbf{x}) \begin{bmatrix} \varepsilon_{11} \\ \varepsilon_{22} \\ 2\varepsilon_{12} \end{bmatrix} + \mathbf{H}(\mathbf{x}) \begin{bmatrix} E_1 \\ E_2 \end{bmatrix} \end{aligned} \quad (8)$$

where

$$\mathbf{C}(\mathbf{x}) = \begin{bmatrix} E_{11}/e & E_{22}v_{12}/e & 0 \\ E_{22}v_{12}/e & E_{22}/e & 0 \\ 0 & 0 & G_{12} \end{bmatrix}$$

with $e = 1 - \frac{E_{22}}{E_{11}}(v_{12})^2$,

in which E_{11} and E_{22} are Young's moduli, G_{12} is the shear modulus, and v_{12} is the Poisson's ratio.

The following essential and natural boundary conditions are assumed for the mechanical field

$$\begin{aligned} u_i(\mathbf{x}) &= \tilde{u}_i(\mathbf{x}), & \text{on } \Gamma_u, \\ t_i(\mathbf{x}) &= \sigma_{ij}n_j = \tilde{t}_i(\mathbf{x}), & \text{on } \Gamma_t, \end{aligned}$$

and for the electrical field

$$\begin{aligned} \psi(\mathbf{x}) &= \tilde{\psi}(\mathbf{x}), & \text{on } \Gamma_p, \\ n_i D_i(\mathbf{x}) &= \tilde{Q}(\mathbf{x}), & \text{on } \Gamma_q, \end{aligned}$$

where Γ_u is the part of the global boundary with prescribed displacements, and on Γ_t , Γ_p and Γ_q the traction vector, the electric potential and the surface charge density are prescribed, respectively.

Instead of writing the global weak-form for the above governing equations, the MLPG method constructs a weak-form over the local fictitious subdomains such as Ω_s , which is a small region taken for each node inside the global domain [Atluri (2004)]. The local subdomains overlap each other, and cover the whole global domain Ω . The local subdomains could be of any geometrical shape and size. In the present paper, the local subdomains are taken to be of a circular shape for simplicity. The local weak-form of the governing equations (1) can be written as

$$\int_{\Omega_s} [\sigma_{ij,j}(\mathbf{x}) + X_i(\mathbf{x})] u_i^*(\mathbf{x}) d\Omega = 0, \quad (9)$$

where $u_i^*(\mathbf{x})$ is a test function.

Using

$$\sigma_{ij,j}u_i^* = (\sigma_{ij}u_i^*)_{,j} - \sigma_{ij}u_{i,j}^*$$

and applying the Gauss divergence theorem to eq. (9) one obtains

$$\int_{\partial\Omega_s} \sigma_{ij}(\mathbf{x})n_j(\mathbf{x})u_i^*(\mathbf{x})d\Gamma - \int_{\Omega_s} \sigma_{ij}(\mathbf{x})u_{i,j}^*(\mathbf{x})d\Omega + \int_{\Omega_s} X_i(\mathbf{x})u_i^*(\mathbf{x})d\Omega = 0, \quad (10)$$

where $\partial\Omega_s$ is the boundary of the local subdomain which consists of three parts $\partial\Omega_s = L_s \cup \Gamma_{st} \cup \Gamma_{su}$ [Atluri (2004)]. Here, L_s is the local boundary that is totally inside the global domain, Γ_{st} is the part of the local boundary which coincides with the global traction boundary, i.e., $\Gamma_{st} = \partial\Omega_s \cap \Gamma_t$, and similarly Γ_{su} is the part of the local boundary that coincides with the global displacement boundary, i.e., $\Gamma_{su} = \partial\Omega_s \cap \Gamma_u$.

By choosing a Heaviside step function as the test function $u_i^*(\mathbf{x})$ in each subdomain

$$u_i^*(\mathbf{x}) = \begin{cases} 1 & \text{at } \mathbf{x} \in \Omega_s \\ 0 & \text{at } \mathbf{x} \notin \Omega_s \end{cases}$$

the local weak-form (10) is converted to the following local boundary-domain integral equations

$$\int_{\partial\Omega_s} t_i(\mathbf{x})d\Gamma + \int_{\Omega_s} X_i(\mathbf{x})d\Omega = 0. \quad (11)$$

Equation (11) is recognized as the overall force equilibrium conditions on the subdomain Ω_s . A pure boundary integral formulation is obtained under the assumption of vanishing body sources. Note that the local integral equations (11) are valid for both homogeneous and nonhomogeneous linear piezoelectric solids. Nonhomogeneous material properties are included in eq. (11) through the elasticity and the piezoelectric tensors in the traction components.

Similarly, the local weak-form of the governing equation (2) can be written as

$$\int_{\Omega_s} D_{j,j}(\mathbf{x})v^*(\mathbf{x})d\Omega = 0, \quad (12)$$

where $v^*(\mathbf{x})$ is a test function.

Applying the Gauss divergence theorem to the local weak-form (12) and choosing the Heaviside step function as the test function $v^*(\mathbf{x})$ one can obtain

$$\int_{L_s + \Gamma_{sp}} Q(\mathbf{x})d\Gamma = - \int_{\Gamma_{sq}} \tilde{Q}(\mathbf{x})d\Gamma, \quad (13)$$

where

$$Q(\mathbf{x}) = D_j n_j = (e_{jkl}u_{k,l} - h_{jk}\psi_{,k})n_j.$$

In the MLPG method the test and the trial functions are not necessarily from the same functional spaces. For internal nodes, the test function is chosen as the Heaviside step function with its support on the local subdomain. The trial functions, on the other hand, are chosen to be the Moving Least-Squares (MLS) approximations by using a number of nodes spread within the domain of influence. The approximated functions for the mechanical displacements and the electric potential can be written as [Atluri (2004)]

$$\mathbf{u}^h(\mathbf{x}) = \Phi^T(\mathbf{x}) \cdot \hat{\mathbf{u}} = \sum_{a=1}^n \phi^a(\mathbf{x})\hat{\mathbf{u}}^a, \quad (14)$$

$$\psi^h(\mathbf{x}) = \sum_{a=1}^n \phi^a(\mathbf{x})\hat{\psi}^a,$$

where the nodal values $\hat{\mathbf{u}}^a$ and $\hat{\psi}^a$ are fictitious parameters for the displacements and the electric potential, respectively, and $\phi^a(\mathbf{x})$ is the shape function associated with the node a . The number of nodes n used for the approximation is determined by the weight function $w^a(\mathbf{x})$. A 4th order spline-type weight function is applied in the present work

$$w^a(\mathbf{x}) = \begin{cases} 1 - 6\left(\frac{d^a}{r^a}\right)^2 + 8\left(\frac{d^a}{r^a}\right)^3 - 3\left(\frac{d^a}{r^a}\right)^4, & 0 \leq d^a \leq r^a \\ 0, & d^a \geq r^a \end{cases}, \quad (15)$$

where $d^a = \|\mathbf{x} - \mathbf{x}^a\|$ and r^a is the size of the support domain. It is seen that the C^1 -continuity is ensured over the entire domain, therefore the continuity conditions of the tractions and the electric charge are satisfied.

The traction vectors $t_i(\mathbf{x})$ at a boundary point $\mathbf{x} \in \partial\Omega_s$ are approximated in terms of the same nodal values $\hat{\mathbf{u}}^a$ as

$$\mathbf{t}^h(\mathbf{x}) = \mathbf{N}(\mathbf{x})\mathbf{C}(\mathbf{x}) \sum_{a=1}^n \mathbf{B}^a(\mathbf{x})\hat{\mathbf{u}}^a + \mathbf{N}(\mathbf{x})\mathbf{L}(\mathbf{x}) \sum_{a=1}^n \mathbf{P}^a(\mathbf{x})\hat{\psi}^a, \quad (16)$$

where the matrix $\mathbf{N}(\mathbf{x})$ is related to the normal vector $\mathbf{n}(\mathbf{x})$ on $\partial\Omega_s$ by

$$\mathbf{N}(\mathbf{x}) = \begin{bmatrix} n_1 & 0 & n_2 \\ 0 & n_2 & n_1 \end{bmatrix},$$

and the matrices \mathbf{B}^a and \mathbf{P}^a are represented by the gradients of the shape functions as

$$\mathbf{B}^a(\mathbf{x}) = \begin{bmatrix} \phi_{,1}^a & 0 \\ 0 & \phi_{,2}^a \\ \phi_{,2}^a & \phi_{,1}^a \end{bmatrix}, \quad \mathbf{P}^a(\mathbf{x}) = \begin{bmatrix} \phi_{,1}^a \\ \phi_{,2}^a \end{bmatrix}.$$

Similarly the electrical charge $Q(\mathbf{x})$ can be approximated by

$$Q^h(\mathbf{x}) = \mathbf{N}_1(\mathbf{x})\mathbf{G}(\mathbf{x}) \sum_{a=1}^n \mathbf{B}^a(\mathbf{x})\hat{\mathbf{u}}^a - \mathbf{N}_1(\mathbf{x})\mathbf{H}(\mathbf{x}) \sum_{a=1}^n \mathbf{P}^a(\mathbf{x})\hat{\psi}^a, \quad (17)$$

where the matrices \mathbf{G} and \mathbf{H} are defined in eq. (8) and

$$\mathbf{N}_1(\mathbf{x}) = [n_1 \quad n_2].$$

Obeying the boundary conditions at those nodal points on the global boundary, where the displacements and the electrical potential are prescribed, and making use of the approximation formula (14), one obtains the discretized form of the boundary conditions as

$$\sum_{a=1}^n \phi^a(\zeta)\hat{\mathbf{u}}^a = \hat{\mathbf{u}}(\zeta) \quad \text{for } \zeta \in \Gamma_u, \quad (18)$$

$$\sum_{a=1}^n \phi^a(\zeta)\hat{\psi}^a = \hat{\psi}(\zeta) \quad \text{for } \zeta \in \Gamma_p. \quad (19)$$

Furthermore, in view of the MLS-approximation (16) and (17) for the unknown quantities in the local boundary-domain integral equations (11) and

(13), we obtain their discretized forms as

$$\begin{aligned} & \sum_{a=1}^n \left(\int_{L_s + \Gamma_{su}} \mathbf{N}(\mathbf{x})\mathbf{C}(\mathbf{x})\mathbf{B}^a(\mathbf{x})d\Gamma \right) \hat{\mathbf{u}}^a \\ & + \sum_{a=1}^n \left(\int_{L_s + \Gamma_{su}} \mathbf{N}(\mathbf{x})\mathbf{L}(\mathbf{x})\mathbf{P}^a(\mathbf{x})d\Gamma \right) \hat{\psi}^a \quad (20) \\ & = - \int_{\Gamma_{st}} \tilde{\mathbf{t}}(\mathbf{x})d\Gamma - \int_{\Omega_s} \mathbf{X}(\mathbf{x})d\Omega, \end{aligned}$$

$$\begin{aligned} & \sum_{a=1}^n \left(\int_{L_s + \Gamma_{sp}} \mathbf{N}_1(\mathbf{x})\mathbf{G}(\mathbf{x})\mathbf{B}^a(\mathbf{x})d\Gamma \right) \hat{\mathbf{u}}^a \\ & - \sum_{a=1}^n \left(\int_{L_s + \Gamma_{sp}} \mathbf{N}_1(\mathbf{x})\mathbf{H}(\mathbf{x})\mathbf{P}^a(\mathbf{x})d\Gamma \right) \hat{\psi}^a \quad (21) \\ & = - \int_{\Gamma_{sq}} \tilde{Q}(\mathbf{x})d\Gamma, \end{aligned}$$

which are considered on the subdomains adjacent to interior nodes as well as to the boundary nodes on Γ_{st} and Γ_{sq} .

3 Local boundary integral equations for 3-D axisymmetric problems

Let us consider a 3-D axisymmetric piezoelectric body generated by the rotation of the planar domain Ω bounded by the boundary Γ around the axis of symmetry as depicted in Fig.1. For axisymmetric problems it is convenient to use cylindrical coordinates (r, φ, z) . The piezoelectric body is assumed to be transversely isotropic with hexagonal symmetry, and the z-axis is oriented in the poling direction. The angular component of the displacements vanishes and all physical field quantities are independent on the angular coordinate φ . In such a case the static equilibrium equations have the following form [Parton and Kudryavtsev (1988)]

$$\begin{aligned} \sigma_{rr,r}(r, z) + \sigma_{rz,z}(r, z) + \frac{1}{r} [\sigma_{rr}(r, z) - \sigma_{\varphi\varphi}(r, z)] \\ = -X_r(r, z), \end{aligned}$$

$$\sigma_{rz,r}(r, z) + \sigma_{zz,z}(r, z) + \frac{1}{r} \sigma_{rz}(r, z) = -X_z(r, z),$$

$$D_{r,r}(r,z) + D_{z,z}(r,z) + \frac{1}{r}D_r(r,z) = 0, \quad (22)$$

where

$$\begin{aligned} \sigma_{rr} &= c_{11}u_{r,r} + c_{13}u_{z,z} + c_{12}\frac{u_r}{r} - e_{31}E_z, \\ \sigma_{zz} &= c_{13}u_{r,r} + c_{13}\frac{u_r}{r} + c_{33}u_{z,z} - e_{33}E_z, \\ \sigma_{\varphi\varphi} &= c_{12}u_{r,r} + c_{11}\frac{u_r}{r} + c_{13}u_{z,z} - e_{31}E_z, \\ \sigma_{rz} &= c_{44}(u_{z,r} + u_{r,z}) - e_{15}E_r, \\ D_r &= e_{15}(u_{z,r} + u_{r,z}) + h_{11}E_r, \\ D_z &= e_{31}u_{r,r} + e_{33}u_{z,z} + e_{31}\frac{u_r}{r} + h_{33}E_z. \end{aligned} \quad (23)$$

In the present analysis, all material parameters in the constitutive equations (23) are considered to be dependent on the (r, z) -coordinates.

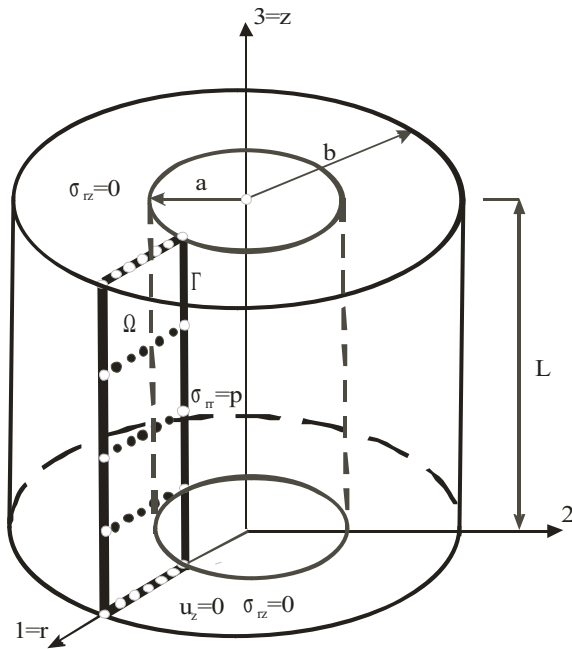


Figure 1: A 3-D axisymmetric body

The local weak-form of the equations (22) on the subdomain Ω_s lying in the global domain Ω can be written as

$$\begin{aligned} \int_{\Omega_s} (\sigma_{rr,r} + \sigma_{rz,z}) u^* d\Omega + \int_{\Omega_s} \frac{1}{r} (\sigma_{rr} - \sigma_{\varphi\varphi}) u^* d\Omega \\ = - \int_{\Omega_s} X_r(r,z) u^* d\Omega, \end{aligned}$$

$$\begin{aligned} \int_{\Omega_s} (\sigma_{zr,r} + \sigma_{zz,z}) v^* d\Omega + \int_{\Omega_s} \frac{1}{r} \sigma_{rz}(r,z) v^* d\Omega \\ = - \int_{\Omega_s} X_z(r,z) v^* d\Omega, \\ \int_{\Omega_s} (D_{r,r} + D_{z,z}) m^* d\Omega + \int_{\Omega_s} \frac{1}{r} D_r m^* d\Omega = 0, \end{aligned} \quad (24)$$

where $u^*(\mathbf{x})$, $v^*(\mathbf{x})$ and $m^*(\mathbf{x})$ are test functions. Applying the Gauss divergence theorem to the first domain integrals of eqs. (24) and selecting Heaviside unit step functions as test functions $u^*(\mathbf{x})$, $v^*(\mathbf{x})$ and $m^*(\mathbf{x})$ in each subdomain like in 2-D problems, one can recast equations (24) into the following form

$$\begin{aligned} \int_{\partial\Omega_s} \sigma_{rb} n_b d\Gamma + \int_{\Omega_s} \frac{1}{r} (\sigma_{rr} - \sigma_{\varphi\varphi}) d\Omega = - \int_{\Omega_s} X_r d\Omega, \\ \int_{\partial\Omega_s} \sigma_{zb} n_b d\Gamma + \int_{\Omega_s} \frac{1}{r} \sigma_{rz} d\Omega = - \int_{\Omega_s} X_z d\Omega, \\ \int_{\partial\Omega_s} D_b n_b d\Gamma + \int_{\Omega_s} \frac{1}{r} D_r d\Omega = 0, \end{aligned} \quad (25)$$

where the subscript b in eq. (25) is considered as a summation index with $b = r, z$.

As in 2-D problems the displacement and the potential fields are approximated by the MLS approximation, and the trial function is specified by the corresponding shape functions. Substituting the approximation formula (14) into the local integral equations (25) a system of linear algebraic equations for the unknown fictitious parameters $\{\hat{u}_r^a, \hat{u}_z^a, \hat{\psi}^a\}$ is obtained as

$$\begin{aligned} \sum_{a=1}^n \hat{u}_r^a \left\{ \int_{\partial\Omega_s} \left[c_{11}n_r\phi_{,r}^a + \frac{c_{12}}{r}n_r\phi^a + c_{44}n_z\phi_{,z}^a \right] d\Gamma \right. \\ \left. + \int_{\Omega_s} \left[\frac{1}{r}(c_{11} - c_{12}) \left(\phi_{,r}^a - \frac{1}{r}\phi^a \right) \right] d\Omega \right\} \\ + \sum_{a=1}^n \hat{u}_z^a \int_{\partial\Omega_s} (c_{13}n_r\phi_{,z}^a + c_{44}n_z\phi_{,r}^a) d\Gamma \end{aligned}$$

$$\begin{aligned}
& + \sum_{a=1}^n \hat{\psi}^a \int_{\partial\Omega_s} (e_{31}n_r\phi_{,z}^a + e_{15}n_z\phi_{,r}^a) d\Gamma \\
& = - \int_{\Omega_s} X_r(r,z) d\Omega,
\end{aligned} \tag{26}$$

$$\begin{aligned}
& \sum_{a=1}^n \hat{u}_z^a \left\{ \int_{\partial\Omega_s} [c_{33}n_z\phi_{,z}^a + c_{44}n_r\phi_{,r}^a] d\Gamma \right. \\
& \quad \left. + \int_{\Omega_s} \frac{c_{44}}{r} \phi_{,r}^a d\Omega \right\} \\
& + \sum_{a=1}^n \hat{u}_r^a \left\{ \int_{\partial\Omega_s} \left(c_{44}n_r\phi_{,z}^a + c_{13}n_z(\phi_{,r}^a + \frac{1}{r}\phi^a) \right) d\Gamma \right. \\
& \quad \left. + \int_{\Omega_s} \frac{c_{44}}{r} \phi_{,z}^a d\Omega \right\} \\
& + \sum_{a=1}^n \hat{\psi}^a \left\{ \int_{\partial\Omega_s} (e_{15}n_r\phi_{,r}^a + e_{33}n_z\phi_{,z}^a) d\Gamma \right. \\
& \quad \left. + \int_{\Omega_s} \frac{1}{r} e_{15}\phi_{,r}^a d\Omega \right\} \\
& = - \int_{\Omega_s} X_z(r,z) d\Omega,
\end{aligned} \tag{27}$$

$$\begin{aligned}
& \sum_{a=1}^n \hat{u}_r^a \left\{ \int_{\partial\Omega_s} \left[e_{15}n_r\phi_{,z}^a + e_{31}n_z(\phi_{,r}^a + \frac{1}{r}\phi^a) \right] d\Gamma \right. \\
& \quad \left. + \int_{\Omega_s} \frac{1}{r} e_{15}\phi_{,z}^a d\Omega \right\} \\
& + \sum_{a=1}^n \hat{u}_z^a \left\{ \int_{\partial\Omega_s} [e_{15}n_r\phi_{,r}^a + e_{33}n_z\phi_{,z}^a] d\Gamma \right. \\
& \quad \left. + \int_{\Omega_s} \frac{1}{r} e_{15}\phi_{,r}^a d\Omega \right\} \\
& - \sum_{a=1}^n \hat{\psi}^a \left\{ \int_{\partial\Omega_s} (h_{11}n_r\phi_{,r}^a + h_{33}n_z\phi_{,z}^a) d\Gamma \right. \\
& \quad \left. + \int_{\Omega_s} \frac{1}{r} h_{11}\phi_{,r}^a d\Omega \right\} \\
& = 0.
\end{aligned}$$

Equations (26)-(28) are considered on the subdomains around each interior node and the boundary nodes on Γ_{st} . On the part of the global boundary Γ_{su} with prescribed displacements and on Γ_{sp} with prescribed potentials the collocation, equations (18) and (19) are applied.

4 Numerical examples

4.1 A central crack in a finite strip

In the first example, a straight central crack in a finite piezoelectric strip under a uniform pure mechanical and/or electrical loading is analyzed. Both loads $\sigma_0 = 1Pa$ and $D_0 = 1C/m^2$ are applied on the top side of the strip, respectively. Due to the bi-axial symmetry of the problem only a quarter of the cracked strip is modeled (Fig. 2). The geometry of the strip resembles the crack problem in an infinite plane in order to utilize the exact solution as a benchmark solution. Thus, the strip width $w = 4a$, crack length $2a = 1.0m$ and strip height $h = w$ are chosen. The mechanical displacements and the electrical potential on the finite strip are approximated by using 930 (31×30) nodes equidistantly distributed. The local subdomains are selected to be circular with a radius $r_{loc} = 0.028m$. To test the accuracy of the present method homogeneous material properties are considered.

The material parameters corresponding to piezoelectric ceramics PZT-4 are given by

$$\begin{aligned}
c_{11} &= 13.9 \cdot 10^{10} Nm^{-2}, & c_{12} &= 7.43 \cdot 10^{10} Nm^{-2}, \\
c_{22} &= 11.5 \cdot 10^{10} Nm^{-2}, & c_{66} &= 2.56 \cdot 10^{10} Nm^{-2}, \\
e_{15} &= 12.7 Cm^{-2}, & e_{21} &= -5.2 Cm^{-2}, \\
e_{22} &= 15.1 Cm^{-2}, \\
h_{11} &= 6.461 \cdot 10^{-9} C(Vm)^{-1}, \\
h_{22} &= 5.62 \cdot 10^{-9} C(Vm)^{-1}.
\end{aligned}$$

For cracks in homogeneous and linear piezoelectric solids the asymptotic behaviour of the field quantities has been given by Sosa (1991) and Pak (1992). In polar coordinates (r, θ) with the origin at the crack-tip, the asymptotic expressions of the

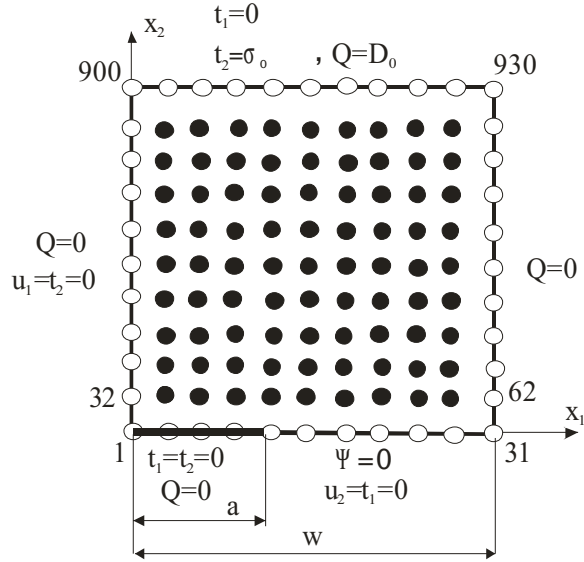


Figure 2: A central crack in a finite piezoelectric strip

electromechanical fields for $r \rightarrow 0$ can be written as

$$\begin{aligned}
 \sigma_{ij}(r, \theta) &= \frac{1}{\sqrt{2\pi r}} \sum_N K_N f_{ij}^N(\theta), \\
 D_i(r, \theta) &= \frac{1}{\sqrt{2\pi r}} \sum_N K_N g_i^N(\theta), \\
 u_i(r, \theta) &= \sqrt{\frac{2r}{\pi}} \sum_N K_N d_i^N(\theta), \\
 \psi(r, \theta) &= \sqrt{\frac{2r}{\pi}} \sum_N K_N v^N(\theta),
 \end{aligned} \quad (29)$$

where $N = I, II, III, IV$, K_I , K_{II} and K_{III} denote the well-known mechanical stress intensity factors (SIF) and K_{IV} is the electrical displacement intensity factor (EDIF). The angular functions $f_{ij}^N(\theta)$, $g_i^N(\theta)$, $d_i^N(\theta)$ and $v^N(\theta)$ are dependent on material properties only and they are given by

$$\begin{aligned}
 f_{i1}^N &= - \sum_{\alpha=1}^4 \operatorname{Re} \left\{ \frac{M_{i\alpha} N_{\alpha N} p_{\alpha}}{\sqrt{\cos \theta + p_{\alpha} \sin \theta}} \right\}, \\
 f_{i2}^N &= \sum_{\alpha=1}^4 \operatorname{Re} \left\{ \frac{M_{i\alpha} N_{\alpha N}}{\sqrt{\cos \theta + p_{\alpha} \sin \theta}} \right\}, \\
 g_1^N &= - \sum_{\alpha=1}^4 \operatorname{Re} \left\{ \frac{M_{4\alpha} N_{\alpha N} p_{\alpha}}{\sqrt{\cos \theta + p_{\alpha} \sin \theta}} \right\},
 \end{aligned}$$

$$g_2^N = \sum_{\alpha=1}^4 \operatorname{Re} \left\{ \frac{M_{4\alpha} N_{\alpha N}}{\sqrt{\cos \theta + p_{\alpha} \sin \theta}} \right\},$$

$$d_i^N = \sum_{\alpha=1}^4 \operatorname{Re} \left\{ A_{i\alpha} N_{\alpha N} \sqrt{\cos \theta + p_{\alpha} \sin \theta} \right\},$$

$$v^N = \sum_{\alpha=1}^4 \operatorname{Re} \left\{ A_{4\alpha} N_{\alpha N} \sqrt{\cos \theta + p_{\alpha} \sin \theta} \right\},$$

where p_{α} are the eigenvalues of the characteristic equation for anisotropic piezoelectric solids and the matrices $A_{i\alpha}$, $M_{i\alpha}$ and $N_{\alpha N}$ can be found in the paper [Park and Sun (1995)]. From equations (29) one can obtain the following expression for the intensity factors [Garcia-Sanchez et al. (2007)]

$$\begin{pmatrix} K_I \\ K_{IV} \end{pmatrix} = \sqrt{\frac{\pi}{8r}} [\operatorname{Re}(\mathbf{B})^{-1}] \begin{pmatrix} \Delta u_2 \\ \Delta \psi \end{pmatrix}, \quad (30)$$

where the matrix \mathbf{B} is determined by the material properties [Garcia-Sanchez et al. (2007)], and the symmetry conditions of the displacements and the potential with respect to the crack plane are utilized.

Ricoeur and Kuna (2003) have obtained a simple expression for the mode-I SIF K_I , which depends on the near field displacement and potential

$$K_I = \sqrt{\frac{\pi}{2r}} \left(\frac{c_T e^2}{c_T \kappa + e^2} u_2 + \frac{c_T \kappa}{c_T \kappa + e^2} \psi \right), \quad (31)$$

where c_T , e and κ are the effective material constants of the simplified Irwin-matrix

$$Y_{MN} = - \sum_{\alpha=1}^4 \operatorname{Re} \{ A_{M\alpha} N_{\alpha N} \}.$$

The extended crack-opening-displacements along the crack are shown in Figs. 3 and 4 for a uniform traction and a uniform electrical displacement loading, respectively. The extended crack-opening-displacements are defined as the differences of the mechanical displacements and the potentials on both crack surfaces. Our numerical results as shown in Figs. 3 and 4 are in very good agreements with the exact closed-form solutions [Pak (1990); Pan (1999)]. Here, one can observe that $\Delta \psi$ caused by a remote stress loading σ_0 is identical to Δu_2 caused by a remote electric displacement loading D_0 as a consequence of the

extended Betti's reciprocal theorem. For a pure positive electrical displacement loading $K_I = 0$, therefore we obtain from eq. (31) a positive crack-opening-displacement Δu_2 and a negative potential jump $\Delta\psi$. It is interesting to note that for a pure mechanical loading, a finite value of the potential jump $\Delta\psi$ on both crack surfaces does not result in a finite value of the EDIF K_{IV} . It means that the crack-opening-displacement Δu_2 and the potential jump $\Delta\psi$ are coupled, but the SIF and the EDIF in this case are uncoupled.

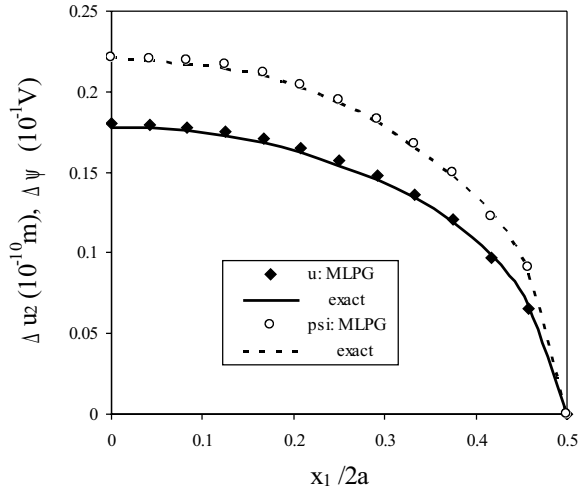


Figure 3: Variations of the crack-opening-displacement and the potential jump with the normalized coordinate $x_1/2a$ for a pure mechanical loading σ_0

For a pure mechanical loading, the computed normalized mode-I SIF is $K_I/\sigma_0\sqrt{\pi a} = 1.01$, which is very close to the exact value $K_I/\sigma_0\sqrt{\pi a} = 1$. A similar accuracy is achieved for a pure electrical displacement loading.

4.2 An edge crack in a finite strip

Next, an edge crack in a finite piezoelectric strip is analyzed. The geometry of the strip is given in Fig. 5 with the following values: $a = 0.5$, $a/w = 0.4$ and $h/w = 4$. Due to the symmetry of the problem with respect to the x_1 -axis, only a half of the strip is modeled. We have used again 930 nodes equidistantly distributed for the MLS approximation of the physical quantities. On the top of the strip either a uniform tension σ_0 , or a

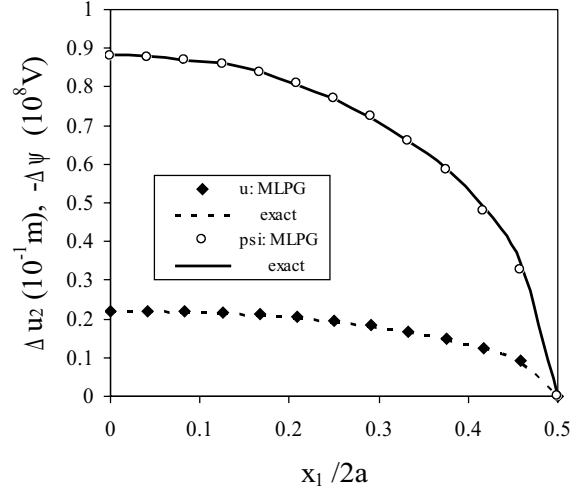


Figure 4: Variations of the crack-opening-displacement and the potential jump with the normalized coordinate $x_1/2a$ for a pure electrical displacement loading D_0

uniform electrical displacement D_0 , or a combination of both loadings is applied. Functionally graded material properties in the x_1 -direction are considered. An exponential variation of the elastic, piezoelectric and dielectric constants is assumed as

$$\begin{aligned} c_{ijkl}(\mathbf{x}) &= c_{ijkl0} \exp(\gamma x_1), \\ e_{ijk}(\mathbf{x}) &= e_{ijk0} \exp(\gamma x_1), \\ h_{ij}(\mathbf{x}) &= h_{ij0} \exp(\gamma x_1), \end{aligned} \quad (32)$$

where c_{ijkl0} , e_{ijk0} and h_{ij0} correspond to the material parameters used in the previous example.

Figures 6 and 7 present the variations of the crack-opening-displacement and the potential jump on the crack surfaces with the x_1 -coordinate for a pure mechanical tension and a pure electric displacement loading, respectively. A value $\gamma = 2$ is assumed for the gradient parameter in the numerical calculations.

Numerical results are given for two different homogeneous materials and for an FGM. One of the homogeneous materials is characterized by the material parameters corresponding to that of the FGM at the left lateral side of the strip $x_1 = 0$. The second one is specified by the material parameters corresponding to that of the FGM with

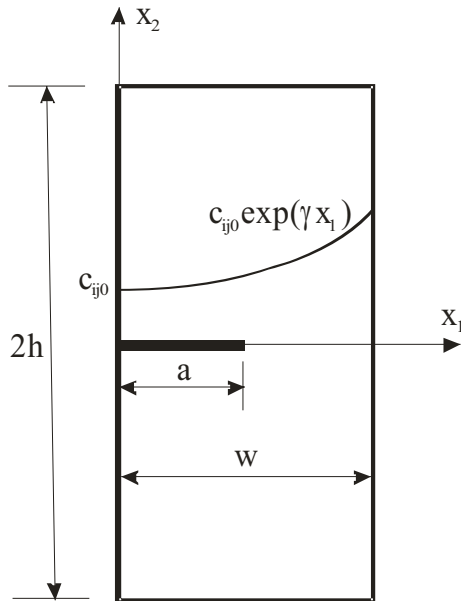


Figure 5: An edge crack in a finite strip with graded material properties in x_1 -direction

$\gamma = 2$ at the crack-tip $x_1 = 0.5$. It follows directly from equation (32) that all material parameters in the second case are e^1 times larger than in the first homogeneous material. One can see that the crack-opening-displacement and potentials are significantly reduced in the second homogeneous material compared to the first one. The boundary value problems have been analyzed also by the FEM computer code ANSYS. There, for the cracked functionally graded piezoelectric strip we have used a multi-layer model consisting of 12 vertical layers with homogeneous material properties in each layer corresponding to that at the center of each layer. Numerical results obtained by the present MLPG and the FEM are in good agreements for both homogeneous and continuously nonhomogeneous piezoelectric materials. The crack-opening-displacements for FGM strip and for homogeneous strip with material parameters corresponding to that of the FGM strip at the crack-tip differ only slightly in the case of a pure mechanical loading. However, for a pure electrical displacement loading the differences between the electrical potential jumps for FGM strip and for homogeneous strip with material parameters corresponding to that of the FGM

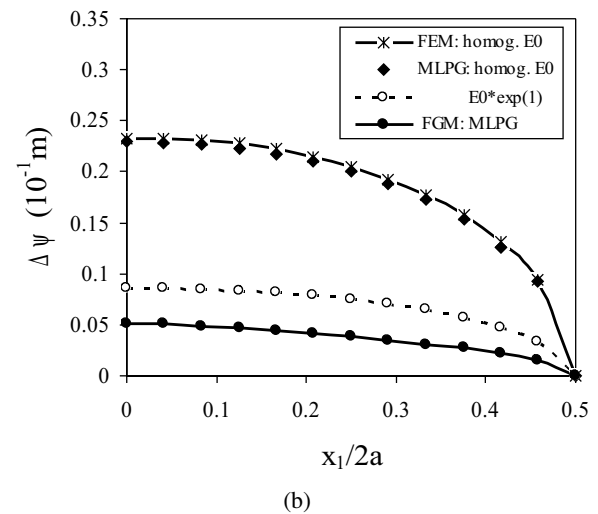
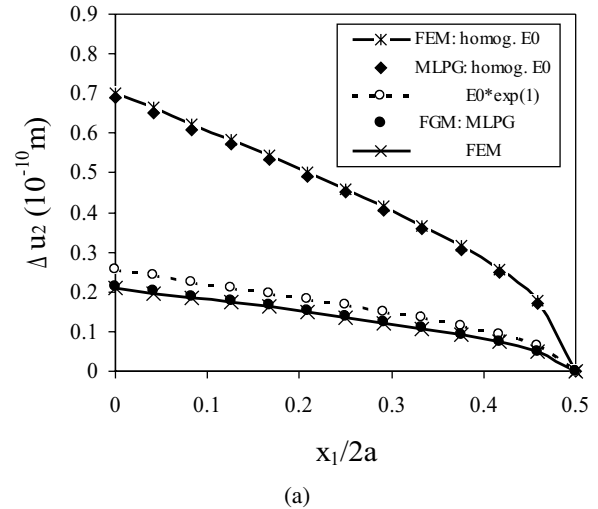


Figure 6: Variations of a) the crack-opening-displacement, and b) potential jump with the normalized coordinate $x_1/2a$ for a pure mechanical loading $\sigma_0 = 1Pa$

strip at the crack-tip are more remarkable (Fig. 7). It means that the gradation of the material parameters has a stronger influence on the electrical potential jump than on the crack-opening-displacement. The variation of the crack opening displacement for a pure electrical load is the same as the variation of potentials for a pure mechanical loading.

Next, we analyze the influence of the material gradation on the stress intensity factor and the electrical displacement intensity factor for an edge cracked strip under a combined load-

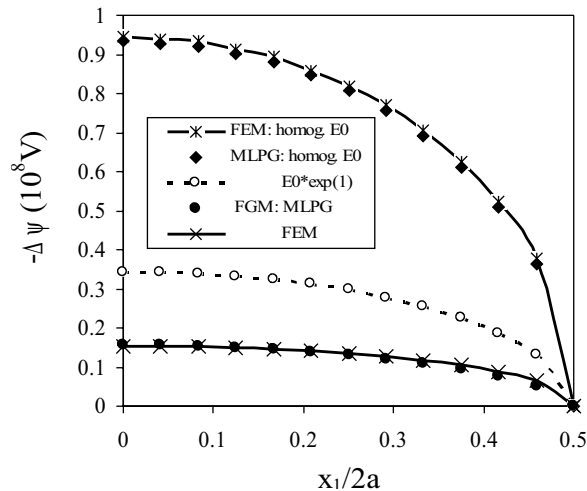


Figure 7: Variation of the potential jump on the crack surfaces with the normalized coordinate $x_1/2a$ for a pure electric displacement loading $D_0 = 1C/m^2$

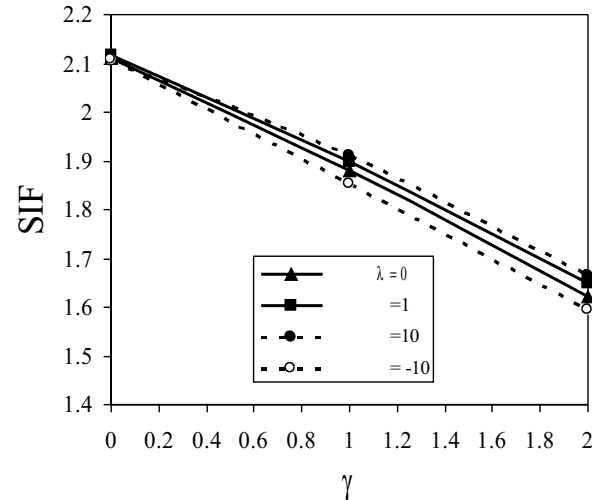


Figure 8: Influence of the material gradation on the stress intensity factor under a combined loading

ing. For convenience, a loading parameter $\lambda = D_{0c220}/(\sigma_0 e_{220})$ is introduced. The variation of the SIF with the gradation exponent γ is presented in Fig. 8. With increasing gradient parameter γ the SIF is decreasing. A similar phenomenon is observed for an edge crack in an elastic FGM strip under a mechanical loading [Dolbow and Gosz (2002)]. For a crack in a homogeneous piezoelectric solid analyzed in the previous example the SIF and the EDIF are uncoupled. However, this conclusion does not valid generally for a continuously nonhomogeneous piezoelectric solid.

Figures 8 and 9 show that in the case of graded material parameters ($\gamma \neq 0$) the stress and the electrical displacement intensity factors are coupled. Different values of the normalized SIF are obtained for various values of λ in the FGM piezoelectric strip. For a homogeneous strip ($\gamma = 0$) one can see that the values of the normalized SIF and EDIF are not dependent on the value of the electrical displacement loading described by λ . All curves in both figures are met at $\gamma = 0$. The coupling is influenced by the loading combination parameter λ . When the magnitude of the applied electric displacement loading (i.e., λ) increases, its influence on the normalized EDIF decreases (see dashed lines in Fig. 9). This means

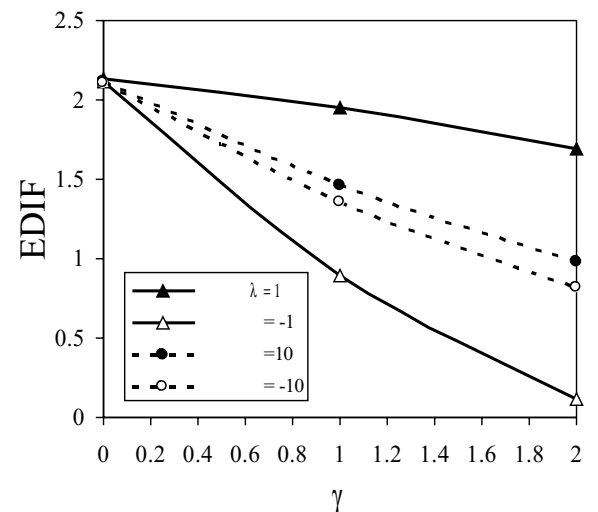


Figure 9: Influence of the material gradation on the electric displacement intensity factor under a combined loading

that the mechanical loading has an insignificant effect on the normalized EDIF $K_{IV}/D_0\sqrt{\pi a}$ under a strong electric loading. The influence of the combined loading on the SIF is weaker than on the EDIF. Similar phenomena were also observed by Chen et al. (2003) for a central crack. However, the SIF and the EDIF increase with increasing gradient parameter for a central crack, which is opposite to the present case for an edge crack.

4.3 A penny-shaped crack in a finite cylinder

A penny-shaped crack in a finite cylinder as depicted in Fig. 10 is analyzed in the third example. The following geometry is considered: crack radius $a = 0.5$, cylinder radius $w = 1.25$, and cylinder length $L = 5.0$. On the top of the cylinder either a uniform tension σ_0 , or a uniform electrical displacement D_0 , or a combination of both loadings is applied.

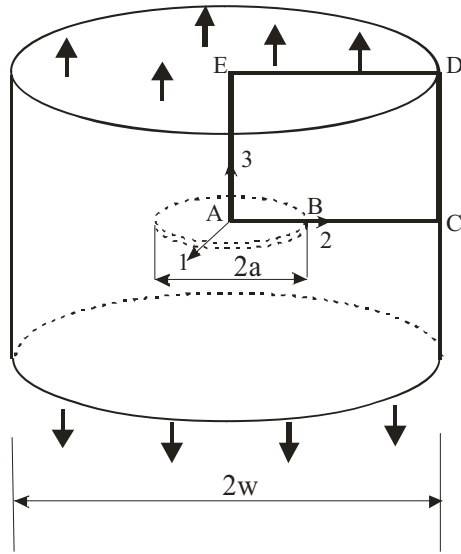


Figure 10: A penny-shaped crack in a finite piezoelectric cylinder

Also in this example, an exponential variation of the elastic, piezoelectric and dielectric constants in radial direction is assumed, i.e.,

$$\begin{aligned} c_{ijkl}(r) &= c_{ijkl0} \exp(\gamma r), \\ e_{ijk}(r) &= e_{ijk0} \exp(\gamma r), \\ h_{ij}(r) &= h_{ij0} \exp(\gamma r). \end{aligned}$$

The material coefficients at the axis of symmetry corresponding to piezoelectric ceramics are given by

$$\begin{aligned} c_{11} &= 13.9 \cdot 10^{10} Nm^{-2}, & c_{13} &= 7.43 \cdot 10^{10} Nm^{-2}, \\ c_{12} &= 7.78 \cdot 10^{10} Nm^{-2}, & c_{33} &= 11.5 \cdot 10^{10} Nm^{-2}, \\ c_{44} &= 2.56 \cdot 10^{10} Nm^{-2}, & c_{22} &= 13.9 \cdot 10^{10} Nm^{-2}, \\ e_{15} &= 12.7 Cm^{-2}, & e_{31} &= -5.2 Cm^{-2}, \\ e_{33} &= 15.1 Cm^{-2}, \end{aligned}$$

$$\begin{aligned} h_{11} &= 6.46 \cdot 10^{-9} C(Vm)^{-1}, \\ h_{33} &= 5.62 \cdot 10^{-9} C(Vm)^{-1}. \end{aligned}$$

Numerical calculations are carried out for several values of the gradient parameter $\gamma = 0., 1., 2.$ A regular node distribution with 930 (31×30) nodes is used for the MLS-approximation of the displacements and the electric potential in the analyzed domain ABCDE (see Fig.10). Fig. 11 shows a comparison of the numerical results for a cracked homogeneous cylinder by the MLPG method and the FEM. One can observe a very good agreement between both results.

The influence of the material gradation on the stress intensity factor and the electrical displacement intensity factor in the cracked cylinder under a combined loading is then analyzed. The combined loading is determined by the parameter $\lambda = D_0 c_{330} / (\sigma_0 e_{330})$ with a uniform tension $\sigma_0 = 1 N/m^2$. In the case of a pure mechanical load ($\lambda = 0$) the piezoelectric constants have no influence on the SIF in a homogeneous cylinder. The variation of the normalized stress intensity factor $f_I = K_I / \sigma_0 \sqrt{\pi a}$ with the gradation exponent γ is presented in Fig. 12. With increasing electrical displacement loading the influence of the material gradation becomes stronger. The normalized electrical displacement intensity factor $K_{IV} / D_0 \sqrt{\pi a}$ is decreasing with increasing gradation exponent γ as shown in Fig.13. The influences of the combined loading on the SIF and the EDIF are almost the same. The differences between the EDIFs (solid lines) for $\lambda = \pm 1$ are larger than that for $\lambda = \pm 10$ (dashed lines).

Finally, Fig. 14 shows the variations of the field intensity factors with the loading combination parameter λ . Numerical results are presented for FGM with the gradient parameter $\gamma = 2$. Here the EDIF is normalized as $K_{IV} / |D_0| \sqrt{\pi a}$. A negative electric displacement loading results in a negative EDIF, while a positive electric displacement loading gives rise to a positive EDIF. Figure 14 implies that the direction of the electric loading has influences on the SIF and the EDIF.

For a pure mechanical loading ($\lambda = 0$) the EDIF is identical zero. For a positive electrical displacement loading ($\lambda > 0$) the potential jump on the

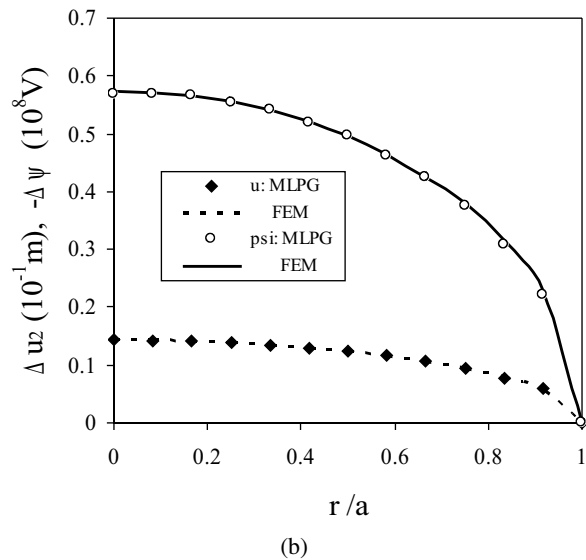
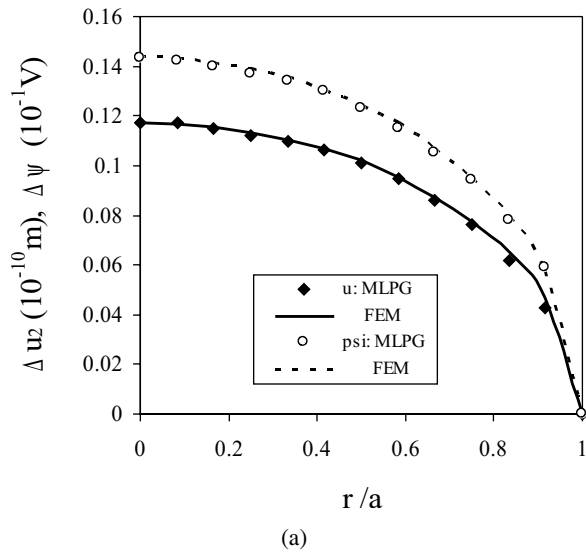


Figure 11: Variations of the crack-opening-displacement and the potential jump with the normalized coordinate r/a for a) a pure mechanical loading σ_0 , and b) a pure electrical displacement loading D_0

crack surfaces is negative and according to eq. (31) the stress intensity factor K_I is reduced. The SIF as shown in Fig. 14 decreases slowly with increasing electrical loading.

5 Conclusions

A meshless local Petrov-Galerkin method (MLPG) is presented for 2-D and 3-D ax-

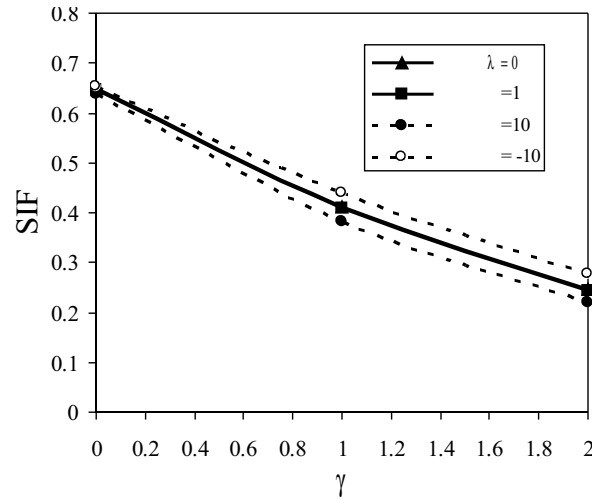


Figure 12: Influence of the material gradation on the SIF for a penny-shaped crack

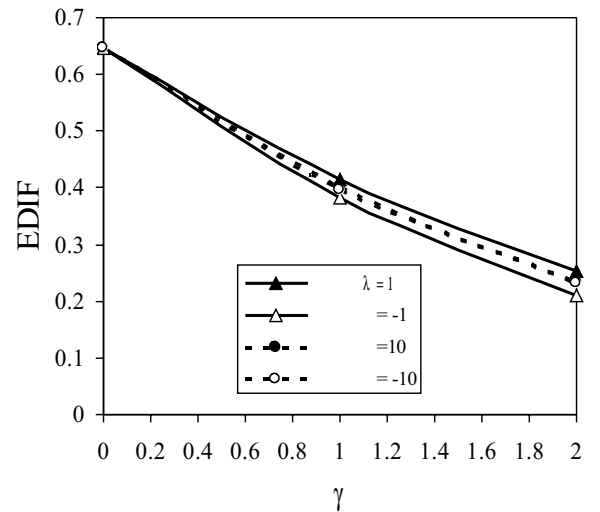


Figure 13: Influence of the material gradation on the EDIF for a penny-shaped crack

isymmetric crack problems in continuously nonhomogeneous and linear piezoelectric solids. The analyzed domain is divided into small overlapping circular subdomains. A unit step function is used as the test functions in the local weak-form of the governing partial differential equations. The derived local boundary-domain integral equations are nonsingular. The Moving Least-Squares (MLS) scheme is adopted for the approximation of the physical field quantities. The proposed method is a truly meshless method,

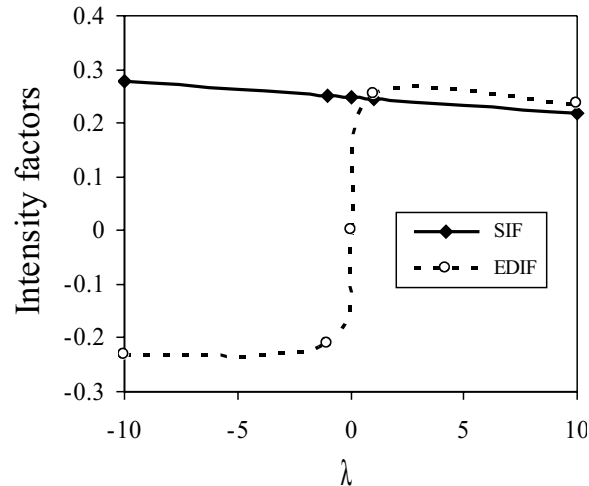


Figure 14: Variations of the SIF and the EDIF with the electrical displacement loading for $\gamma = 2$

which requires neither domain elements nor background cells in either the interpolation or the integration.

The present method provides an alternative numerical tool to many existing computational methods like the FEM or the BEM. The main advantage of the present method is its simplicity. Contrary to the conventional BEM, the present method requires no fundamental solutions and all integrands in the present formulation are regular. Thus, no special numerical techniques are required to evaluate the integrals. It should be noted here that the fundamental solutions are not available for piezoelectric solids with continuously varying material properties in general cases. The present formulation possesses the generality of the FEM. Therefore, the method is promising for numerical analysis of multi-field problems like piezoelectric or thermoelastic problems, which cannot be solved efficiently by the conventional BEM. Moreover, the present meshless method is more flexible with respect to the adaptation, since an adaptation of the nodal density is easier than a mesh adaptation.

An essential drawback of the present method is its larger computing time in comparison with the conventional domain-type discretization methods such as the FEM. The main reason is the fact that a meshless approximation usually involves more

nodes and the required shape functions are more complex. To reduce the computing time, a mixed formulation [Atluri et al. (2006)] can be applied, which reduces the radius of the support domain at the same accuracy as in the traditional approximation. Since a smaller size of the support domain decreases the bandwidth of the system matrix, the computing time can be significantly reduced. Therefore, future research efforts will be devoted to developing efficient approaches for the present meshless method to reduce its computing time.

Acknowledgement: The authors acknowledge the support by the Slovak Science and Technology Assistance Agency registered under number APVV-20-035404, the Slovak Grant Agency VEGA-2/6109/6, and the German Research Foundation (DFG) under the project number ZH 15/6-1.

References

- Atluri, S.N.** (2004): *The Meshless Method, (MLPG) For Domain & BIE Discretizations*, Tech Science Press.
- Atluri, S.N.; Sladek, J.; Sladek, V.; Zhu, T.** (2000): The local boundary integral equation (LBIE) and its meshless implementation for linear elasticity. *Comput. Mech.*, 25: 180-198.
- Atluri, S.N.; Han, Z.D.; Shen, S.** (2003): Meshless local Petrov-Galerkin (MLPG) approaches for solving the weakly-singular traction & displacement boundary integral equations. *CMES: Computer Modeling in Engineering & Sciences*, 4: 507-516.
- Atluri, S.N.; Liu, H.T.; Han, Z.D.** (2006): Meshless local Petrov-Galerkin (MLPG) mixed finite difference method for solid mechanics. *CMES: Computer Modeling in Engineering & Sciences*, 15: 1-16.
- Belytschko, T.; Krogauz, Y.; Organ, D.; Fleming, M.; Krysl, P.** (1996): Meshless methods; an overview and recent developments. *Comp. Meth. Appl. Mech. Engrn.*, 139: 3-47.
- Chen, J.; Liu, Z.X.; Zou, Z.Z.** (2003): Electromechanical impact of a crack in a functionally

graded piezoelectric medium. *Theoretical and Applied Fracture Mechanics*, 39: 47-60.

Davi, G.; Milazzo, A. (2001): Multidomain boundary integral formulation for piezoelectric materials fracture mechanics. *Int. J. Solids Structures*, 38: 2557-2574.

Dolbow, J.E.; Gosz, M. (2002): On computation of mixed-mode stress intensity factors in functionally graded materials. *Int. J. Solids Structures*, 39: 7065-7078.

Enderlein, M.; Ricoeur, A.; Kuna, M. (2005): Finite element techniques for dynamic crack analysis in piezoelectrics. *International Journal of Fracture*, 134: 191-208.

Garcia-Sanchez, F.; Saez, A.; Dominguez, J. (2005): Anisotropic and piezoelectric materials fracture analysis by BEM. *Computers & Structures*, 83: 804-820.

Garcia-Sanchez, F.; Zhang, Ch.; Sladek, J.; Sladek, V. (2007): 2-D transient dynamic crack analysis in piezoelectric solids by BEM. *Computational Materials Science*, 39: 179-186.

Govorukha, V.; Kamlah, M. (2004): Asymptotic fields in the finite element analysis of electrically permeable interfacial cracks in piezoelectric bimaterials. *Archives of Applied Mechanics*, 74: 92-101.

Gruebner, O.; Kamlah, M.; Munz, D. (2003): Finite element analysis of cracks in piezoelectric materials taking into account the permittivity of the crack medium. *Eng. Fracture Mechanics*, 70: 1399-1413.

Gross, D.; Rangelov, T.; Dineva, P. (2005): 2D wave scattering by a crack in a piezoelectric plane using traction BIEM. *SID: Structural Integrity & Durability*, 1: 35-47.

Gross, D.; Dineva, P.; Rangelov, T. (2007): BIEM solution for piezoelectric cracked finite solids under time-harmonic loading. *Eng. Anal. with Boundary Elements*, 31: 152-162.

Han, F.; Pan, E.; Roy, A.K.; Yue, Z.Q. (2006): Responses of piezoelectric, transversely isotropic, functionally graded and multilayered half spaces to uniform circular surface loading. *CMES: Computer Modeling in Engineering & Sciences*, 14:

15-30.

Han, Z.D.; Atluri, S.N. (2004a): Meshless local Petrov-Galerkin (MLPG) approaches for solving 3D problems in elasto-statics. *CMES: Computer Modeling in Engineering & Sciences*, 6: 169-188.

Han, Z.D.; Atluri, S.N. (2004b): A meshless local Petrov-Galerkin (MLPG) approach for 3-dimensional elasto-dynamics. *CMC: Computers, Materials & Continua*, 1: 129-140.

Kuna, M. (1998): Finite element analyses of crack problems in piezoelectric structures. *Computational Materials Science*, 13: 67-80.

Kuna, M. (2006): Finite element analyses of cracks in piezoelectric structures – a survey. *Archives of Applied Mechanics*, 76:725-745.

Liu, G.R.; Dai, K.Y.; Lim, K.M.; Gu, Y.T. (2002): A point interpolation mesh free method for static and frequency analysis of two-dimensional piezoelectric structures. *Computational Mechanics*, 29: 510-519.

Ohs, R.R.; Aluru, N.R. (2001): Meshless analysis of piezoelectric devices. *Computational Mechanics*, 27: 23-36.

Pan, E. (1999): A BEM analysis of fracture mechanics in 2D anisotropic piezoelectric solids. *Engineering Analysis with Boundary Elements*, 23: 67-76.

Pak, Y.E. (1990): Crack extension force in a piezoelectric material. *ASME J. Applied Mechanics*, 57: 647-653.

Pak, Y.E. (1992): Linear electro-elastic fracture mechanics of piezoelectric materials. *International Journal of Fracture*, 54: 79-100.

Park, S.B.; Sun, C.T. (1995): Effect of electric field on fracture of piezoelectric ceramics. *International Journal of Fracture*, 70: 203-216.

Parton, V.Z.; Kudryavtsev, B.A. (1988): *Electromagnetoelasticity, Piezoelectrics and Electrically Conductive Solids*, Gordon and Breach Science Publishers, New York.

Parton, V.Z.; Kudryavtsev, B.A.; Senik, N.A. (1989): Electroelasticity. *Applied Mechanics, Soviet Review*, 2: 1-58.

Paulino, G.H.; Jin, Z.H.; Dodds, R.H. (2003): Failure of functionally graded materials. In: Kar-

ihaloo B, Knauss WG, editors, Comprehensive Structural Integrity, Volume 2, Elsevier Science, 607-644.

Rajapakse, R.K.N.D.; Xu, X.L. (2001): Boundary element modeling of cracks in piezoelectric solids. *Engineering Analysis with Boundary Elements*, 25: 771-781.

Ricoeur, A.; Kuna, M. (2003): Influence of electric fields on the fracture of ferroelectric ceramics. *Journal of the European Ceramic Society*, 23: 1313-1328.

Saez, A.; Garcia-Sanchez, F.; Dominguez, J. (2006): Hypersingular BEM for dynamic fracture in 2-D piezoelectric solids. *Comput. Meth. Appl. Mech. Eng.*, 196: 235-246.

Sellountos, E.J.; Vavourakis, V.; Polyzos, D. (2005): A new singular/hypersingular MLPG (LBIE) method for 2D elastostatics. *CMES: Computer Modeling in Engineering & Sciences*, 7: 35-48.

Sheng, N.; Sze, K.Y. (2006): Multi-region Trefftz boundary element method for fracture analysis in plane piezoelectricity. *Computational Mechanics*, 37: 381-393.

Shindo, Y.; Narita, F.; Tanaka, K. (1996): Electroelastic intensification near anti-plane shear crack in orthotropic piezoelectric ceramic strip. *Theoretical and Applied Fracture Mechanics*, 25: 65-71.

Shindo, Y.; Tanaka, K.; Narita, F. (1997): Singular stress and electric fields of a piezoelectric ceramic strip with a finite crack under longitudinal shear. *Acta Mechanica*, 120: 31-45.

Sladek, J.; Sladek, V.; Atluri, S.N. (2000): Local boundary integral equation (LBIE) method for solving problems of elasticity with nonhomogeneous material properties. *Computational Mechanics*, 24: 456-462.

Sladek, J.; Sladek, V.; Atluri, S.N. (2004): Meshless local Petrov-Galerkin method in anisotropic elasticity. *CMES: Computer Modeling in Engineering & Sciences*, 6: 477-489.

Sladek, J.; Sladek, V.; Zhang, Ch.; Garcia-Sanchez, F.; Wünsche, M. (2006): Meshless Local Petrov-Galerkin Method for Plane Piezoelec-

tricity. *CMC: Computers, Materials & Continua*, 4: 109-118.

Sosa, H. (1991): Plane problems in piezoelectric media with defects. *Int. J. Solids Structures*, 28: 491-505.

Suresh, S.; Mortensen, A. (1998): Fundamentals of Functionally Graded Materials, Institute of Materials, London.

Ueda, S. (2003): Crack in functionally graded piezoelectric strip bonded to elastic surface layers under electromechanical loading. *Theoretical and Applied Fracture Mechanics*, 40: 225-236.

Yang, J.H.; Lee, K.Y. (2001): Penny shaped crack in a three-dimensional piezoelectric strip under in-plane normal loadings. *Acta Mechanica*, 148: 187-197.

Zhu, T.; Zhang, J.D.; Atluri, S.N. (1998): A local boundary integral equation (LBIE) method in computational mechanics, and a meshless discretization approach. *Computational Mechanics*, 21: 223-235.

Zhu, X.; Wang, Z.; Meng, A. (1995): A functionally gradient piezoelectric actuator prepared by metallurgical process in PMN-PZ-PT system. *J. Mater. Sci. Lett.*, 14: 516-518.

Zhu, X.; Zhu, J.; Zhou, S.; Li, Q.; Liu, Z. (1999): Microstructures of the monomorph piezoelectric ceramic actuators with functionally gradient. *Sensors Actuators A*, 74: 198-202.